Computer Assisted Mechanics and Engineering Sciences, 8: 439–453, 2001.

A posteriori error estimation for equilibrium finite elements in elastostatic problems

Orlando J.B. Almeida Pereira and José P. Moitinho de Almeida
Departamento de Engenharia Civil e Arquitectura,
Instituto Superior Técnico, Universidade Técnica de Lisboa,
Av. Rovisco Pais, 1049-001 Lisboa, Portugal

(Received June 30, 2000)

Equilibrated solutions, locally satisfying all the equilibrium conditions, may be obtained by using a special case of the hybrid finite element formulation. Equilibrium finite element solutions will normally present compatibility defaults, which may be directly used to estimate the error of the solution, *a posteriori*. Another approach is to construct a compatible solution using the stresses and displacements available from the hybrid solution. From this dual solution, an upper bound for the global error is obtained. In this paper, the hybrid equilibrium element formulation, the occurrence of spurious kinematic modes and the use of super-elements, in *2D* and *3D*, are briefly reviewed. Compatibility defaults for *2D* and *3D* are presented, together with an expression for an element error indicator explicitly based on such defaults. A local procedure for recovering conforming displacements from the equilibrium finite element solution is also presented. The *h*-refinement procedure is adapted to prevent irregular refinement patterns.

1. Introduction

Equilibrium finite elements have been used, since 1964 [18], to obtain equilibrated solutions, locally satisfying all the equilibrium conditions. These elements may be obtained by using a special case of the hybrid finite element formulation [1, 2]. When linear approximation functions are used for the stresses, hybrid equilibrium elements are also a special case of hybrid Trefftz elements [5].

Strong enforcement of co-diffusivity on the sides may cause the occurrence of spurious kinematic modes. These may be prevented by assembling the elements into super-elements [19].

Equilibrium finite element solutions will normally present compatibility defaults [12, 14, 15]. These defaults may be directly used to estimate the error of the solution, *a posteriori*. Another approach is to construct a compatible solution using the stresses and displacements available from the hybrid solution [10, 12, 14, 15]. From this dual solution, an upper bound for the global error is obtained [4, 17].

In this paper, the hybrid equilibrium element formulation, the occurrence of spurious kinematic modes and the use of super-elements, in *2D* and *3D*, will be briefly reviewed. Compatibility defaults for *2D* and *3D* will be presented, together with an expression for an element error indicator explicitly based on such defaults. A local procedure for recovering conforming displacements from the equilibrium finite element solution will also be presented. Numerical results for self-adaptive refinement in a simple plane stress problem will close the paper.

2. Basic equations

We shall consider a *2D* or *3D* domain Ω, with boundary Γ. On the kinematic boundary, Γ_u, the displacements are imposed,

$$\boldsymbol{u} = \boldsymbol{u}_\Gamma \,. \tag{1}$$

The strains are obtained from the displacements, using the compatibility differential operator,

$$\boldsymbol{\varepsilon} = \boldsymbol{d}\boldsymbol{u}. \tag{2}$$

In linear elasticity, the relation between the strains and the stresses is

$$\boldsymbol{\varepsilon} = \boldsymbol{f}\boldsymbol{\sigma}. \tag{3}$$

Equilibrium between the stresses and the body forces is expressed by

$$\boldsymbol{d}^T\boldsymbol{\sigma} + \boldsymbol{f} = 0. \tag{4}$$

On the static boundary, Γ_t, the tractions are imposed,

$$\boldsymbol{N}\boldsymbol{\sigma} = \boldsymbol{t}_\Gamma\,. \tag{5}$$

3. Hybrid equilibrium finite element formulation

In this section, we shall describe the hybrid equilibrium formulation. We will follow Almeida and Freitas [1] and Almeida and Pereira [2].

The stress field inside element i is approximated as

$$\boldsymbol{\sigma}_{e,(i)} = \boldsymbol{S}_{(i)}\hat{\boldsymbol{s}}_{(i)} + \boldsymbol{\sigma}_{0,(i)}\,. \tag{6}$$

To ensure equilibrium inside the elements, the approximation functions that are linearly combined are chosen so that

$$\boldsymbol{d}^T\boldsymbol{S}_{(i)} = \boldsymbol{0} \tag{7}$$

and the particular solution is chosen so that

$$\boldsymbol{d}^T\boldsymbol{\sigma}_{0,(i)} + \boldsymbol{f} = \boldsymbol{0}. \tag{8}$$

To ensure invariance with respect to the coordinate system, complete sets of polynomials are used for stress approximation functions.

The displacements are separately approximated on each side j as

$$\boldsymbol{v}_{e,(j)} = \boldsymbol{V}_{(j)}\hat{\boldsymbol{v}}_{(j)} + \bar{\boldsymbol{v}}_{(j)}\,. \tag{9}$$

In this equation, if $\Gamma_{(j)} \subset \Gamma_u$, $\boldsymbol{v}_{e,(j)} = \bar{\boldsymbol{v}}_{(j)} = \boldsymbol{u}_\Gamma$; if $\Gamma_{(j)} \not\subset \Gamma_u$, $\bar{\boldsymbol{v}}_{(j)} = \boldsymbol{0}$.

Interelement equilibrium on side j is enforced, using the displacement approximation functions as weighing functions, by

$$\sum_i \left(\int_{\Gamma_{(j)}} \boldsymbol{V}_{(j)}^T\,\boldsymbol{N}_{(j),(i)}\,\boldsymbol{S}_{(i)}\,\mathrm{d}\Gamma\right)\hat{\boldsymbol{s}}_{(i)} = \int_{\Gamma_{(j)}} \boldsymbol{V}_{(j)}^T\,\bar{\boldsymbol{t}}_{(j)}\,\mathrm{d}\Gamma - \sum_i \left(\int_{\Gamma_{(j)}} \boldsymbol{V}_{(j)}^T\,\boldsymbol{N}_{(j),(i)}\,\boldsymbol{\sigma}_{0,(i)}\,\mathrm{d}\Gamma\right),$$

$$\text{or} \qquad \sum_i \boldsymbol{D}_{(j),(i)}\,\hat{\boldsymbol{s}}_{(i)} = \hat{\bar{\boldsymbol{t}}}_{(j)} - \sum_i \hat{\boldsymbol{t}}_{0,(j),(i)}\,. \tag{10}$$

For each element i, the weighted residual form of compatibility equation (2) results in

$$-\left(\int_{\Omega_{(i)}} \boldsymbol{S}_{(i)}^T\,\boldsymbol{f}\,\boldsymbol{S}_{(i)}\,\mathrm{d}\Omega\right)\hat{\boldsymbol{s}}_{(i)} + \sum_j \left(\int_{\Gamma_{(j)}} \boldsymbol{S}_{(i)}^T\,\boldsymbol{N}_{(j),(i)}^T\,\boldsymbol{V}_{(j)}\,\mathrm{d}\Gamma\right)\hat{\boldsymbol{v}}_{(j)}$$

$$= \int_{\Omega_{(i)}} \boldsymbol{S}_{(i)}^T\,\boldsymbol{f}\boldsymbol{\sigma}_{0,(i)}\,\mathrm{d}\Omega - \sum_j \int_{\Gamma_{(j)}} \boldsymbol{S}_{(i)}^T\,\boldsymbol{N}_{(j),(i)}^T\,\bar{\boldsymbol{v}}_{(j)}\,\mathrm{d}\Gamma,$$

$$\text{or} \qquad -\boldsymbol{F}_{(i)}\,\hat{\boldsymbol{s}}_{(i)} + \sum_i \boldsymbol{D}_{(j),(i)}^T\,\hat{\boldsymbol{v}}_{(j)} = \hat{\boldsymbol{e}}_{0,(i)} - \sum_i \hat{\bar{\boldsymbol{v}}}_{(i),(j)}\,. \tag{11}$$

The global algebraic system is obtained by assembling the compatibility equations of all finite elements and the equilibrium equations of all sides that do not belong to the kinematic boundary. Assembling the element and side matrices or vectors into global ones, the algebraic system may be written as

$$\begin{bmatrix} -\boldsymbol{F} & \boldsymbol{D}^T \\ \boldsymbol{D} & \boldsymbol{0} \end{bmatrix} \begin{bmatrix} \hat{\boldsymbol{s}} \\ \hat{\boldsymbol{v}} \end{bmatrix} = \begin{bmatrix} \hat{\boldsymbol{e}}_0 - \hat{\bar{\boldsymbol{v}}} \\ \hat{\bar{\boldsymbol{t}}} - \hat{\boldsymbol{t}}_0 \end{bmatrix}. \tag{12}$$

4. Spurious modes and super-elements

Complete sets of polynomials are also used for the displacement approximation functions on the sides. For displacement approximation functions whose degree is equal to that of the stress approximation functions in the elements and not inferior to that of $\boldsymbol{\sigma}_{0,(i)}$, or $\boldsymbol{t}_\Gamma$, equilibrium of tractions on the sides is locally enforced by Eq. (10), provided that the sides have linear parametric representation.

When equilibrium is strongly enforced on the sides, the global system in Eq. (12) may be impossible or underdetermined. Nevertheless, when a solution for the stress field exists, it is unique. Only the side displacements may be affected by spurious kinematic modes.

Simplicial elements minimise the number of spurious kinematic modes at element level. The number of these modes is given in Table 1. The numbers given for *2D* by Veubeke [19] were proved by Maunder and Almeida [9]. The numbers given for *3D* [12, 15] have been verified for $p \leq 4$.

Table 1. Number of spurious kinematic modes for a simplicial element of degree p

p	Triangle	Tetrahedron
0	0	0
1	2	9
≥ 2	3	$6(p+1)$

Most of these spurious modes are not present when a mesh is assembled, although new global modes may appear. When the equations are consistent and a solution exists, a solver that can provide one of the solutions of an underdetermined system may be used.

Using special assemblies of simplicial elements, super-elements, ensures that spurious kinematic modes are either completely absent or internal to the super-elements. Therefore, a solution is always possible.

For $p \geq 1$, meshes of simplicial super-elements are free from spurious kinematic modes [19]. These super-elements are shown in Figure 1, for *2D* and *3D*.

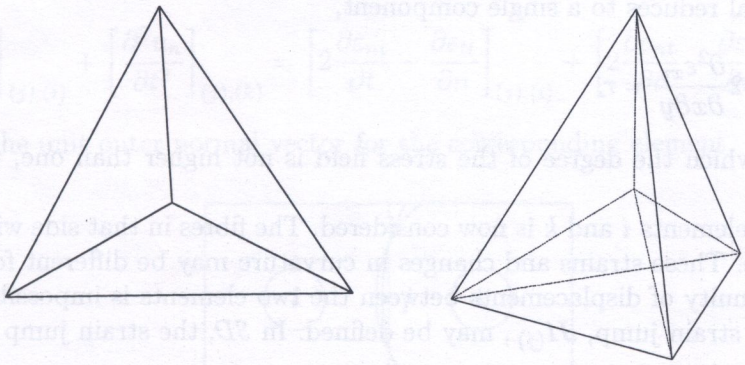

Fig. 1. Simplicial super-elements, for *2D* and *3D*

5. COMPATIBILITY DEFAULTS

Unless the exact solution can be represented by the approximation functions used for the stresses in the equilibrium finite element model, the corresponding strains will not satisfy locally the compatibility conditions and there will be an error in the finite element solution. Therefore, compatibility defaults may be defined, both inside the elements and on the element sides.

Inside the elements, the lack of compatibility can be measured by the residual in the StVenant compatibility equations.

In *3D*, this residual is a fourth order tensor, $\boldsymbol{r}$, with 81 components,

$$\frac{\partial^2 \varepsilon_{ij}}{\partial x_k \partial x_l} - \frac{\partial^2 \varepsilon_{ki}}{\partial x_l \partial x_j} + \frac{\partial^2 \varepsilon_{lk}}{\partial x_j \partial x_i} - \frac{\partial^2 \varepsilon_{jl}}{\partial x_i \partial x_k} = r_{ijkl} \,. \tag{13}$$

From these components, 27 are always null, 12 are equal to

$$\frac{\partial^2 \varepsilon_{xy}}{\partial x \partial z} - \frac{\partial^2 \varepsilon_{xx}}{\partial z \partial y} + \frac{\partial^2 \varepsilon_{zx}}{\partial y \partial x} - \frac{\partial^2 \varepsilon_{yz}}{\partial x^2} = r_{xyxz} \,, \tag{14}$$

12 are equal to

$$\frac{\partial^2 \varepsilon_{yx}}{\partial y \partial z} - \frac{\partial^2 \varepsilon_{yy}}{\partial z \partial x} + \frac{\partial^2 \varepsilon_{zy}}{\partial x \partial y} - \frac{\partial^2 \varepsilon_{yz}}{\partial y^2} = r_{yxyz} \,, \tag{15}$$

12 are equal to

$$\frac{\partial^2 \varepsilon_{xz}}{\partial y \partial z} - \frac{\partial^2 \varepsilon_{yx}}{\partial z^2} + \frac{\partial^2 \varepsilon_{zy}}{\partial z \partial x} - \frac{\partial^2 \varepsilon_{zz}}{\partial x \partial y} = r_{xzyz} \,, \tag{16}$$

6 are equal to

$$\frac{\partial^2 \varepsilon_{xx}}{\partial y^2} + \frac{\partial^2 \varepsilon_{yy}}{\partial x^2} - 2\frac{\partial^2 \varepsilon_{xy}}{\partial x \partial y} = r_{xxyy} \,, \tag{17}$$

6 are equal to

$$\frac{\partial^2 \varepsilon_{xx}}{\partial z^2} + \frac{\partial^2 \varepsilon_{zz}}{\partial x^2} - 2\frac{\partial^2 \varepsilon_{xz}}{\partial x \partial z} = r_{xxzz} \,, \tag{18}$$

and 6 are equal to

$$\frac{\partial^2 \varepsilon_{yy}}{\partial z^2} + \frac{\partial^2 \varepsilon_{zz}}{\partial y^2} - 2\frac{\partial^2 \varepsilon_{yz}}{\partial y \partial z} = r_{yyzz} \,. \tag{19}$$

In 2D, the residual reduces to a single component,

$$\frac{\partial^2 \varepsilon_{xx}}{\partial y^2} + \frac{\partial^2 \varepsilon_{yy}}{\partial x^2} - 2\frac{\partial^2 \varepsilon_{xy}}{\partial x \partial y} = r. \tag{20}$$

For elements in which the degree of the stress field is not higher than one, these residuals are always zero.

A side j between elements i and k is now considered. The fibres in that side will have strains and changes in curvature. These strains and changes in curvature may be different for each element, in which case the continuity of displacements between the two elements is impossible [12, 14, 15].

For each side j, a strain jump, $\boldsymbol{J1}_{(j)}$, may be defined. In *3D*, the strain jump is the tensor

$$\boldsymbol{J1}_{(j)} = \begin{bmatrix} \varepsilon_{t_1 t_1} & \varepsilon_{t_1 t_2} \\ \varepsilon_{t_2 t_1} & \varepsilon_{t_2 t_2} \end{bmatrix}_{(j),(i)} - \begin{bmatrix} \varepsilon_{t_1 t_1} & \varepsilon_{t_1 t_2} \\ \varepsilon_{t_2 t_1} & \varepsilon_{t_2 t_2} \end{bmatrix}_{(j),(k)} , \tag{21}$$

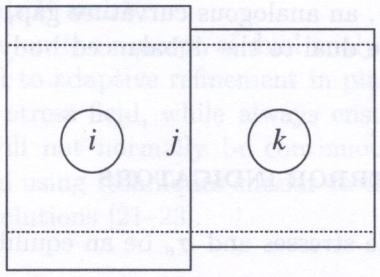

Fig. 2. Strain jump of side j between elements i and k

where $\boldsymbol{t}_1$ and $\boldsymbol{t}_2$ are orthogonal unit vectors in the plane that is tangent to the side. In *2D*, as shown in Fig. 2, the strain jump reduces to [20]

$$\boldsymbol{J1}_{(j)} = [\varepsilon_{tt}]_{(j),(i)} - [\varepsilon_{tt}]_{(j),(k)} \,, \tag{22}$$

where $\boldsymbol{t} = [-n_y \; n_x]^T$ is the unit vector tangent to the side.

On the kinematic boundary Γ_u, an analogous strain gap, ***G1***, may be defined.

For the same generic side, a curvature jump, $\boldsymbol{J2}_{(j)}$, may also be defined. In *3D*, the curvature jump is the tensor

$$\boldsymbol{J2}_{(j)} = \left[\begin{array}{cc} \dfrac{\partial^2 u_n}{\partial t_1^2} & \dfrac{\partial^2 u_n}{\partial t_1 \partial t_2} \\ \dfrac{\partial^2 u_n}{\partial t_2 \partial t_1} & \dfrac{\partial^2 u_n}{\partial t_2^2} \end{array}\right]_{(j),(i)} + \left[\begin{array}{cc} \dfrac{\partial^2 u_n}{\partial t_1^2} & \dfrac{\partial^2 u_n}{\partial t_1 \partial t_2} \\ \dfrac{\partial^2 u_n}{\partial t_2 \partial t_1} & \dfrac{\partial^2 u_n}{\partial t_2^2} \end{array}\right]_{(j),(k)} , \tag{23}$$

which may also be written as

$$\boldsymbol{J2}_{(j)} = \left[\begin{array}{cc} 2\dfrac{\partial \varepsilon_{nt_1}}{\partial t_1} - \dfrac{\partial \varepsilon_{t_1 t_1}}{\partial n} & \dfrac{\partial \varepsilon_{nt_1}}{\partial t_2} + \dfrac{\partial \varepsilon_{nt_2}}{\partial t_1} - \dfrac{\partial \varepsilon_{t_1 t_2}}{\partial n} \\ \dfrac{\partial \varepsilon_{nt_1}}{\partial t_2} + \dfrac{\partial \varepsilon_{nt_2}}{\partial t_1} - \dfrac{\partial \varepsilon_{t_1 t_2}}{\partial n} & 2\dfrac{\partial \varepsilon_{nt_2}}{\partial t_2} - \dfrac{\partial \varepsilon_{t_2 t_2}}{\partial n} \end{array}\right]_{(j),(i)}$$

$$+ \left[\begin{array}{cc} 2\dfrac{\partial \varepsilon_{nt_1}}{\partial t_1} - \dfrac{\partial \varepsilon_{t_1 t_1}}{\partial n} & \dfrac{\partial \varepsilon_{nt_1}}{\partial t_2} + \dfrac{\partial \varepsilon_{nt_2}}{\partial t_1} - \dfrac{\partial \varepsilon_{t_1 t_2}}{\partial n} \\ \dfrac{\partial \varepsilon_{nt_1}}{\partial t_2} + \dfrac{\partial \varepsilon_{nt_2}}{\partial t_1} - \dfrac{\partial \varepsilon_{t_1 t_2}}{\partial n} & 2\dfrac{\partial \varepsilon_{nt_2}}{\partial t_2} - \dfrac{\partial \varepsilon_{t_2 t_2}}{\partial n} \end{array}\right]_{(j),(k)} , \tag{24}$$

In these expressions, $\boldsymbol{n}$ is the unit outer normal vector for the corresponding element.

In *2D*, as shown in Fig. 3, the curvature jump reduces to [20]

$$\boldsymbol{J2}_{(j)} = \left[\frac{\partial^2 u_n}{\partial t^2}\right]_{(j),(i)} + \left[\frac{\partial^2 u_n}{\partial t^2}\right]_{(j),(k)} = \left[2\frac{\partial \varepsilon_{nt}}{\partial t} - \frac{\partial \varepsilon_{tt}}{\partial n}\right]_{(j),(i)} + \left[2\frac{\partial \varepsilon_{nt}}{\partial t} - \frac{\partial \varepsilon_{tt}}{\partial n}\right]_{(j),(k)} , \tag{25}$$

where again $\mathbf{n}$ is the unit outer normal vector for the corresponding element.

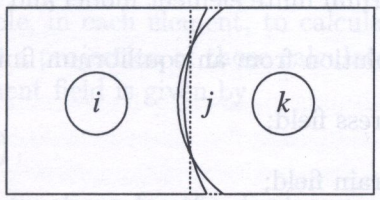

Fig. 3. Curvature jump of side j between elements i and k

On the kinematic boundary Γ_u, an analogous curvature gap, ***G2***, may be defined.

These compatibility defaults are dual to the unbalanced body forces and the traction jumps for compatible finite elements [3, 7].

6. Error estimators and error indicators

Let $\boldsymbol{\sigma}$ be the exact solution for the stresses and $\boldsymbol{\sigma}_e$ be an equilibrium finite element solution. The error in the stress field is

$$\boldsymbol{e}_e = \boldsymbol{\sigma} - \boldsymbol{\sigma}_e \,. \tag{26}$$

The strain energy norm of the error in each finite element is

$$\|\boldsymbol{e}_e\|_{E,(i)} = \left(\int_{\Omega_{(i)}} (\boldsymbol{\sigma} - \boldsymbol{\sigma}_e)^T f (\boldsymbol{\sigma} - \boldsymbol{\sigma}_e) \, \mathrm{d}\Omega \right)^{\frac{1}{2}} . \tag{27}$$

The global strain energy norm of the error is

$$\|\boldsymbol{e}_e\|_E = \left(\sum_{i=1}^{NE} \|\boldsymbol{e}_e\|^2_{E,(i)} \right)^{\frac{1}{2}} . \tag{28}$$

An error estimator ϵ is an estimate of the global strain energy norm of the error $\|\boldsymbol{e}_e\|_E$. If the estimated error exceeds the required tolerance, it will be reduced by refining the finite element discretization. Using adaptive refinement, the required accuracy will be obtained at a minimal cost. Adaptive refinement is guided by the error indicators $\epsilon_{(i)}$ which provide the contribution of each element to the approximation of the global error. The error estimator is then defined by

$$\epsilon = \left(\sum_{i=1}^{NE} \epsilon^2_{(i)} \right)^{\frac{1}{2}} . \tag{29}$$

The quality of an error estimator is usually measured by its effectivity index [7]

$$\theta = \frac{\epsilon}{\|\boldsymbol{e}\|_E} . \tag{30}$$

An error estimator is asymptotically exact if $\theta \to 1$ when $h \to 0$ or $p \to \infty$. The error estimator will be an upper bound of the error if $\theta \geq 1$.

7. Error indicators for equilibrium elements

Several methods may be used to obtain error indicators for an equilibrium finite element solution, among which [12, 15]:

I. Parallel analysis of an equilibrium finite element model and a compatible finite element model;

II. Derivation of a compatible solution from an equilibrium finite element solution;

III. Derivation of a continuous stress field;

IV. Derivation of a continuous strain field;

V. Explicit use of the compatibility defaults.

This paper will focus on methods II and V.

The first two methods are based on the concept of dual analysis, which will be described in the next section. Method I was applied to adaptive refinement in plane elasticity by Pereira [12].

The equilibrium finite element stress field, while always ensuring the equilibrium of tractions on the sides between elements, will not normally be continuous. The continuous fields used in methods III and IV may be derived using techniques similar to those used for smoothing the stress field of compatible finite element solutions [21–23].

8. Dual analysis

Let $\boldsymbol{u}_c$ be a compatible displacement field, with an error $\boldsymbol{e}_c$, and $\boldsymbol{\sigma}_e$ be an equilibrated stress field, with an error $\boldsymbol{e}_e$. Then, [4],

$$U(\boldsymbol{\sigma}_e - \boldsymbol{\sigma}_c) = \pi_P(\boldsymbol{u}_c) + \pi_C(\boldsymbol{\sigma}_e), \tag{31}$$

and, [17],

$$U(\boldsymbol{e}_e) + U(\boldsymbol{e}_c) = U(\boldsymbol{\sigma}_e - \boldsymbol{\sigma}_c). \tag{32}$$

Therefore, for either field, dual analysis yields an upper bound of the global error,

$$\|\boldsymbol{e}\|_E \leq \epsilon = \|\boldsymbol{\sigma}_e - \boldsymbol{\sigma}_c\|_E \,. \tag{33}$$

This value, $\|\boldsymbol{\sigma}_e - \boldsymbol{\sigma}_c\|_E$, can be interpreted as an error in the constitutive relation [8].

For a given finite element mesh, this upper bound may be computed from the error indicators

$$\epsilon_{(i)} = \|\boldsymbol{\sigma}_e - \boldsymbol{\sigma}_c\|_{E,(i)} \,. \tag{34}$$

In Method I, both $\boldsymbol{\sigma}_e$ and $\boldsymbol{u}_c$ are finite element solutions [11, 13], which may be computed in parallel. In Method II, $\boldsymbol{\sigma}_e$ is an equilibrium finite element solution and $\boldsymbol{u}_c$ is a compatible displacement field derived from the equilibrium finite element solution and the kinematic boundary conditions, as described in the next section.

9. Derivation of a compatible displacement field from an equilibrium finite element solution

A finite element solution obtained using equilibrium elements of degree p yields, for each side j, a displacement field $\boldsymbol{v}_{e,(j)}$ of degree p.

A compatible displacement field may be derived, from the equilibrium finite element solution and the kinematic boundary conditions. This is achieved by calculating a displacement field that is continuous within each element and then by making this field compatible on the whole domain and on the kinematic boundary [12, 14, 15]. This procedure is dual to that of the Ladevèze approach [8] for recovering an equilibrated stress field from a compatible finite element solution.

If $p \leq 1$, the strains computed from the discretized stresses correspond to a displacement field which is continuous within each element but is normally discontinuous across the sides. If $p > 1$, normally it is not possible to obtain a displacement field, within each element, for which the strains will match exactly those computed from the stress field.

Nevertheless, it is always possible, in each element, to calculate a displacement field of degree $p+1$, $\boldsymbol{u}_e$, for which the strains are a projection of those calculated from a stress field of degree p.

In each element i, the displacement field is given by

$$\boldsymbol{u}_{e,(i)} = \boldsymbol{\Psi}_{(i)} \left(\hat{\boldsymbol{u}}_{S,(i)} + \boldsymbol{R}_{(i)} \, \hat{\boldsymbol{u}}_{R,(i)} \right), \tag{35}$$

where $\boldsymbol{\Psi}_{(i)}$ are the approximation functions for the displacements and $\boldsymbol{R}_{(i)}$ transforms the rigid body movement amplitudes $\hat{\boldsymbol{u}}_{R,(i)}$ into displacement parameters.

The deformed shape of an element, as described by $\boldsymbol{\Psi}_{(i)}\hat{\boldsymbol{u}}_{S,(i)}$, is computed to within a rigid body movement from

$$\left(\int_{\Omega_{(i)}} (\boldsymbol{d}\boldsymbol{\Psi}_{(i)})^T \boldsymbol{f}^{-1} (\boldsymbol{d}\boldsymbol{\Psi}_{(i)})\, \mathrm{d}\Omega\right) \hat{\boldsymbol{u}}_{S,(i)} = \int_{\Omega_{(i)}} (\boldsymbol{\partial}\boldsymbol{\Psi})^T \boldsymbol{\sigma}_{e,(i)}\, \mathrm{d}\Omega. \tag{36}$$

This system has six dependant equations in *3D* and three in *2D*, respectively, corresponding to the rigid body movement. The displaced position of the element may be calculated from the side displacements, when spurious kinematic modes are not present. In this case, a least squares solution to the local overdetermined system formed by equations

$$\left(\int_{\Gamma_{(j)}} \boldsymbol{\Psi}_{(i)}\, \mathrm{d}\Gamma\right) \left(\hat{\boldsymbol{u}}_{S,(i)} + \boldsymbol{R}_{(i)}\, \hat{\boldsymbol{u}}_{R,(i)}\right) = \int_{\Gamma_{(j)}} \boldsymbol{v}_{e,(j)}\, \mathrm{d}\Gamma, \tag{37}$$

for each side j of element i, provides the amplitudes $\hat{\boldsymbol{u}}_{R,(i)}$ of the rigid body movement.

As both $\boldsymbol{\sigma}_e$ and $\boldsymbol{v}_e$ correspond to the same equilibrium finite element solution, some of the equations in system (37), respectively six in *3D* and three in *2D*, are dependant. Therefore, for tetrahedral and triangular elements, all the equations in system (37) are consistent and have an unique solution for $\hat{\boldsymbol{u}}_{R,(i)}$.

For triangular elements, a system without redundant equations is formed by equations

$$\left(\int_{\Gamma_{(j)}} \boldsymbol{t}^T_{(j),(i)}\, \boldsymbol{\Psi}_{(i)}\, \mathrm{d}\Gamma\right) \left(\hat{\boldsymbol{u}}_{S,(i)} + \boldsymbol{R}_{(i)}\, \hat{\boldsymbol{u}}_{R,(i)}\right) = \int_{\Gamma_{(j)}} \boldsymbol{t}^T_{(j),(i)}\, \boldsymbol{v}_{e,(j)}\, \mathrm{d}\Gamma, \tag{38}$$

for each side j of element i.

The displacement field $\boldsymbol{u}_e$ is normally discontinuous across the sides and does not satisfy the kinematic boundary conditions. A compatible displacement field of degree $p+1$, $\boldsymbol{u}_c$, may be obtained by smoothing the displacements $\boldsymbol{u}_e$ and enforcing the kinematic boundary conditions. Simple nodal averaging was used but several of the more sophisticated methods used for stress smoothing [21–23] may also be adapted for smoothing displacements.

This method of obtaining an error estimator provides an upper bound of the error and a compatible displacement field. It is better suited to meshes of triangular and tetrahedral super-elements, where no spurious kinematic modes are present.

This method was applied by May [10] to error estimation for uniform meshes of triangular super-elements of degree one.

10. Explicit use of the compatibility defaults

An element error indicator that explicitly uses the previously defined compatibility defaults is expressed by [12, 14, 15]

$$\begin{aligned}\epsilon^2_{(i)} = {} & c_1\, a\, h^4_{(i)}\, \|\boldsymbol{r}\|^2_{I,(i)} + c_2\, a \sum_j \left(h_{(j)} \left\|\frac{1}{2}\boldsymbol{J1}\right\|^2_{I,(j)}\right) + c_2\, a \sum_k \left(h_{(k)}\, \|\boldsymbol{G1}\|^2_{I,(k)}\right) \\ & + c_3\, a \sum_j \left(h^3_{(j)} \left\|\frac{1}{2}\boldsymbol{J2}\right\|^2_{I,(j)}\right) + c_3\, a \sum_k \left(h^3_{(k)}\, \|\boldsymbol{G2}\|^2_{I,(k)}\right),\end{aligned} \tag{39}$$

where the sums in j include all the sides belonging to the boundary of element i, but not to the boundary of Ω and the sums in k include the sides of element i that belong to the kinematic boundary. In this expression, it is assumed that $\boldsymbol{J1}_{(j)}$ and $\boldsymbol{J2}_{(j)}$ are equally divided between the two elements connected by side j. To ensure the correct dimensionality, coefficients c_1, c_2 and c_3 are non-dimensional, a has the dimensions of a stress and h has the dimension of a length.

The norms used in (39) should be invariant.

The norms proposed in [12, 15] for *3D* were

$$\|\boldsymbol{r}\|^2_{I,(i)} = \int_{\Omega_{(i)}} (2r^2_{xyxz} + 2r^2_{xyyz} + 2r^2_{xzyz} + r^2_{xxyy} + r^2_{xxzz} + r^2_{yyzz})\,\mathrm{d}\Omega, \tag{40}$$

and

$$\left\|\frac{1}{2}\boldsymbol{J1}\right\|^2_{I,(j)} = \frac{1}{4}\int_{\Gamma_{(j)}} (J1^2_{t_1t_1} + 2J1^2_{t_1t_2} + J1^2_{t_2t_2})\,\mathrm{d}\Gamma. \tag{41}$$

The definitions of $\|\frac{1}{2}\boldsymbol{J2}\|^2_{I,(j)}$, $\|\boldsymbol{G1}\|^2_{I,(k)}$ and $\|\boldsymbol{G2}\|^2_{I,(k)}$ are analogous to (41). All of these are invariant.

The norms used in [12, 14, 15] for *2D* were

$$\|\boldsymbol{r}\|^2_{I,(i)} = \int_{\Omega_{(i)}} r^2\,\mathrm{d}\Omega, \tag{42}$$

and

$$\left\|\frac{1}{2}\boldsymbol{J1}\right\|^2_{I,(j)} = \frac{1}{4}\int_{\Gamma_{(j)}} (J1_{tt})^2\,\mathrm{d}\Gamma. \tag{43}$$

The definitions of $\|\frac{1}{2}\boldsymbol{J2}\|^2_{I,(j)}$, $\|\boldsymbol{G1}\|^2_{I,(k)}$ and $\|\boldsymbol{G2}\|^2_{I,(k)}$ are analogous to (43).

For coefficient a, the proposed values were $E(1-\nu)/((1+\nu)(1-2\nu))$ for three-dimensional elasticity and plane strain and $E/(1-\nu^2)$ for plane stress. In this way, for given exact and approximate strain fields, ϵ^2 is a linear function of E and its variation with ν corresponds to what is obtained in the case of simple strain ($\varepsilon_{xx} \neq 0$, $\varepsilon_{yy} = \varepsilon_{xy} = 0$).

For the terms corresponding to $\boldsymbol{J1}_{(j)}$ and $\boldsymbol{G1}_{(k)}$, $h_{(j)} = V_{(i)}/A_{(j)}$ was used, which is proportional to the "height" of the element, when generalised "areas" and "volumes" are used. For the terms corresponding to $\boldsymbol{J2}_{(j)}$ and $\boldsymbol{G2}_{(k)}$, $h^3_{(j)} = V_{(i)}A^{3-D}_{(j)}$ was used, where D=2 for plane problems and D=3 for solids.

For triangular elements in adaptively refined meshes, the values of the non-dimensional coefficients used in [12, 14, 15] are shown in Table 2. These values were determined by numerical experimentation and cannot be considered as fit for universal use.

Table 2. Non-dimensional coefficients for the error indicators.

degree	c_1	c_2	c_3
1	-	1.67×10^{-1}	1.66×10^{-2}
2	1.03×10^{-3}	2.03×10^{-1}	0
3	1.48×10^{-4}	7.78×10^{-2}	2.56×10^{-6}

For some examples, sequences of adaptively refined meshes were generated using the mesh generator described in [16]. The elements were always triangular and not assembled into super-elements. The error indicators obtained using compatible displacement elements of higher degree and the error estimator obtained by applying an extrapolation scheme [12] to both sequences of equilibrium and displacement solutions were taken as "exact". The values of the coefficients were obtained from a least squares fit of the error indicators followed by a least squares fit of the error estimators.

This method of obtaining an error estimator avoids the need to derive a compatible displacement field and is independent of the presence of spurious kinematic modes. The error estimator may be above or below the exact value.

11. Improvement of asymptotically non-exact error estimators

For any equilibrated finite element solution,

$$U(\boldsymbol{e}_e) = \pi_C(\sigma_e) - \pi_C(\sigma). \tag{44}$$

Using the effectivity index defined in (30),

$$\epsilon^2 = \theta^2[\pi_C(\sigma_e) - \pi_C(\sigma)]. \tag{45}$$

Assuming that θ is the same for two successive solutions [15],

$$\tilde{\theta}_n = \left(\frac{\epsilon_{n-1}^2 - \epsilon_n^2}{\pi_C(\sigma_{e,n-1}) - \pi_C(\sigma_{e,n})}\right)^{\frac{1}{2}}. \tag{46}$$

Then, an improved error estimator is

$$\tilde{\epsilon}_n = \frac{\epsilon_n}{\tilde{\theta}_n}. \tag{47}$$

The improved estimate may no longer be an upper bound.

This method may only be applied to formulations in which the energy of the error is equal to the error in the energy. The improvement depends on the variation of θ, but not on the value of θ itself. There will be a considerable improvement if θ is high but constant for successive solutions.

12. Numerical examples

The techniques described in the previous sections are exemplified for the cantilever shown in Fig. 4, modelled as a plane stress problem. The eight elements shown in the same Figure are either primitive elements with quadratic approximation functions or super-elements with linear approximation functions. This mesh will also be used as the initial mesh for h-adaptive refinement procedures.

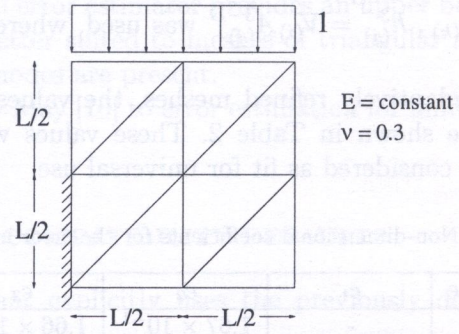

Fig. 4. Cantilever and initial mesh

The h-refinement will be performed by successively dividing each element or super-element into 4, until the new mesh has the required refinement level at each vertex of the current mesh [16]. The hybrid finite element formulation allows for the use of meshes with irregular vertices, since the elements may have any number of sides. Details of the adaptive strategy are given in [12, 15].

The adaptive procedures used in this section will differ in the method used to compute the error indicators. These procedures are the following:

a) use super-elements with linear approximation functions and derive a compatible quadratic displacement field from the equilibrated solution, as in Section 9, to be used as dual solution, as in Section 8;

b) use primitive elements with quadratic approximation functions and compute the error indicators from the compatibility defaults, as in Section 10.

In Procedure a), the derivation of the compatible displacement field, for the initial mesh, is illustrated in Fig. 5.

Since the side displacements obtained from the hybrid model are of the same degree as the stress approximation, the discontinuities at the vertices in Fig. 5(a) cannot be reliably used to indicate the solution error.

The deformed shapes in Fig. 5(b) were obtained from Eq. (36), using a complete quadratic basis as the approximation functions $\Psi_{(i)}$ for the displacements in each primitive element. The rigid body movements were obtained from the side displacements in Figure 5(a), using Eq. (38).

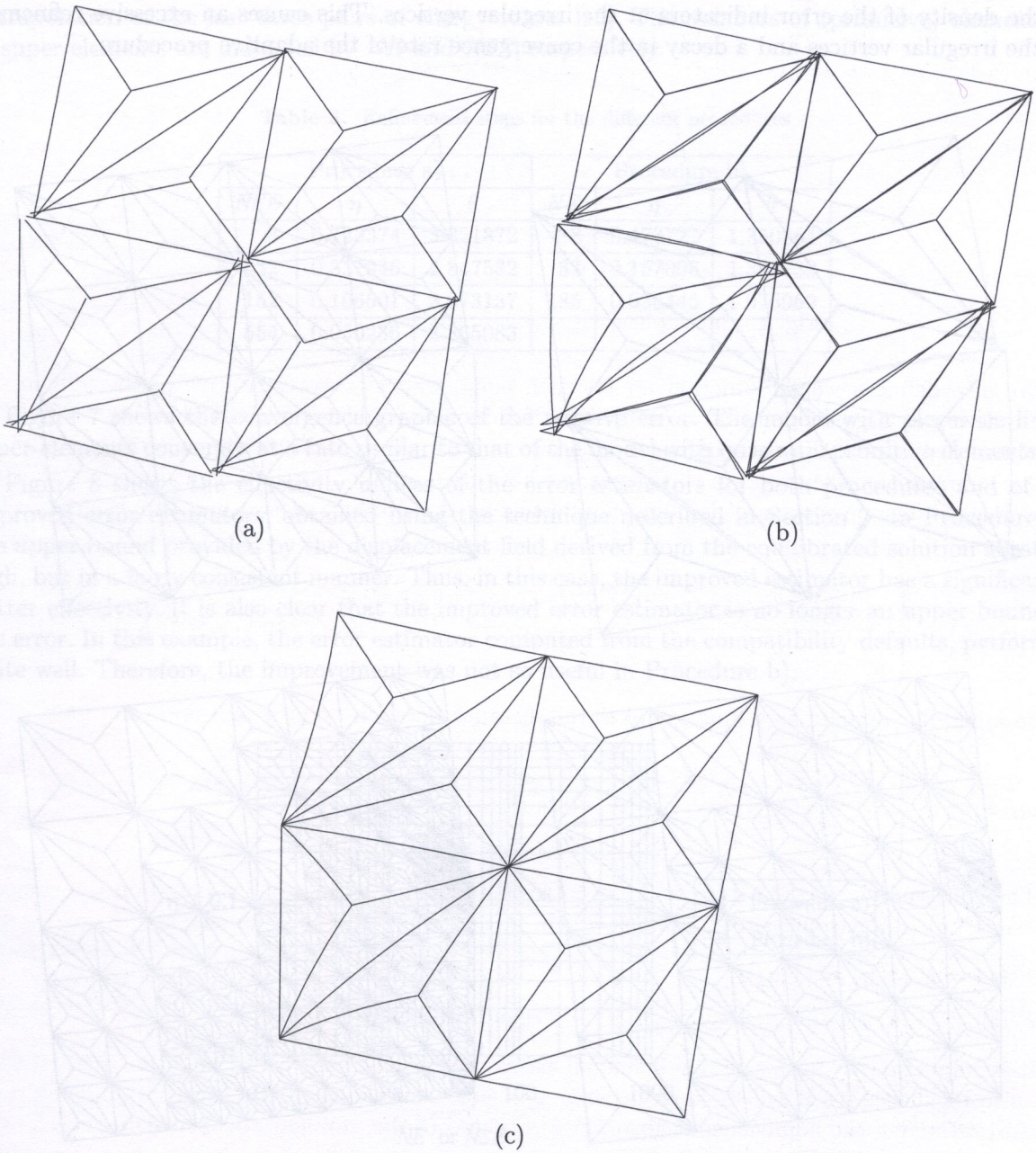

Fig. 5. Derivation of the compatible solution, for the initial mesh in Procedure a)

In this case, since the stress field in each primitive element is linear, the compatibility residual in Eq. (20) is zero. Therefore, within each primitive element, the strains corresponding to the displacement field in Fig. 5(b) will match exactly those computed from the stress field. As a consequence, the discontinuities in the displacement field will also match the strain and curvature defaults computed as defined in Section 5. For elements of higher degree this would not, in general, be the case.

The compatible displacement field shown in Fig. 5(c) was obtained by averaging the vertex and mid-side displacements in Fig. 5(b) and enforcing the kinematic boundary conditions.

This process may easily be generalised for meshes with any number of irregular vertices between two regular vertices of an element. No spurious kinematic modes are introduced since an irregular side of a super-element is always a regular side of another super-element.

However, the analysis of this example in [15] shows that if the number of irregular vertices between two regular vertices of an element becomes high, the quality of the smoothed displacements will eventually decay. This leads to a worse effectivity ratio for the error estimator and to high variations of the density of the error indicators at the irregular vertices. This causes an excessive refinement at the irregular vertices and a decay in the convergence rate of the adaptive procedure.

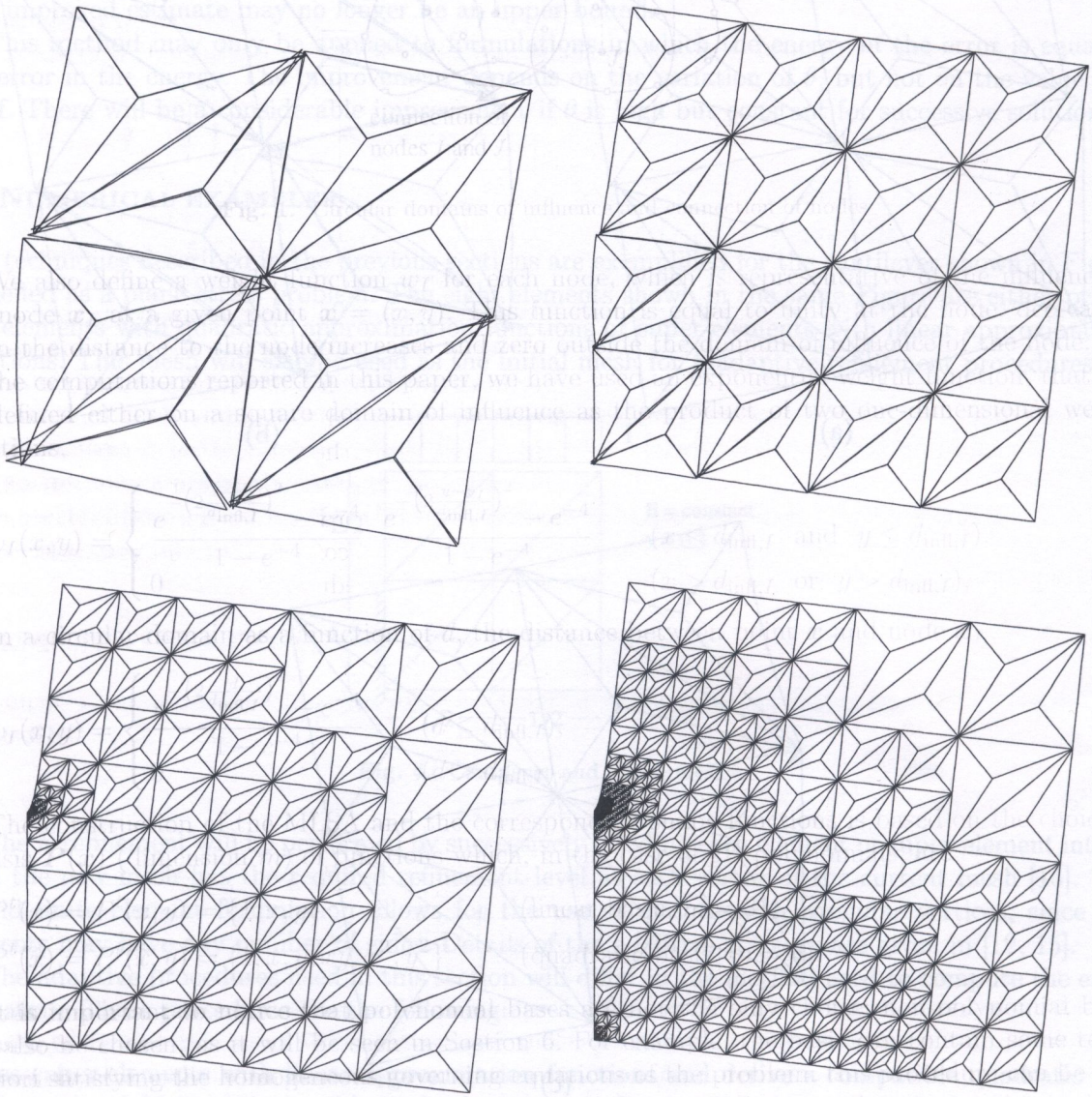

Fig. 6. Element displacements, before smoothing, for Procedure a)

To avoid this problem, the number of irregular vertices between two regular ones is now limited. A unique value of the required refinement level at each vertex is used for all adjacent elements and the value of the required refinement level at an irregular vertex is limited by the minimum value among those at the neighbouring regular vertices.

The incompatible displacement fields for the successive refinement steps in Procedure a) are shown in Fig. 6.

In Procedure b), there is no need to limit the number of irregular vertices between two regular ones, since there does not seem to be any danger of excessive refinement at the irregular vertices when the error indicators are computed from the compatibility defaults.

Table 3 shows the values of the "exact" relative errors $\eta = \|\boldsymbol{e}_e\|/\|\boldsymbol{u}\|$ and of the corresponding effectivity index $\eta = \epsilon/\|\boldsymbol{e}_e\|$, during both adaptive procedures. The "exact" errors were computed with reference to a very accurate solution obtained by a parallel analysis of an equilibrium finite element model and a compatible finite element model, both of fourth degree, followed by a dual extrapolation of the last three pairs of energy values [12]. The numbers of (primitive) elements or of super-elements are indicated by *NE* and *NSE*, respectively.

Table 3. Refinement steps for the different procedures

Procedure a)			Procedure b)		
NSE	η	θ	*NE*	η	θ
8	0.723374	3.321872	8	0.473727	1.350864
32	0.337946	2.847582	38	0.157006	1.345739
152	0.106501	2.673137	185	0.036445	1.076969
554	0.030236	2.865083			

Figure 7 shows the convergence graphic of the relative error. The model with piecewise linear super-elements converges at a rate similar to that of the model with quadratic primitive elements [6].

Figure 8 shows the effectivity indices of the error estimators for both procedures and of the improved error estimators, obtained using the technique described in Section 7. In Procedure a), the upper bound provided by the displacement field derived from the equilibrated solution is rather high, but in a fairly consistent manner. Thus, in this case, the improved estimator has a significantly better effectivity. It is also clear that the improved error estimator is no longer an upper bound of the error. In this example, the error estimator computed from the compatibility defaults, performed quite well. Therefore, the improvement was not so useful in Procedure b).

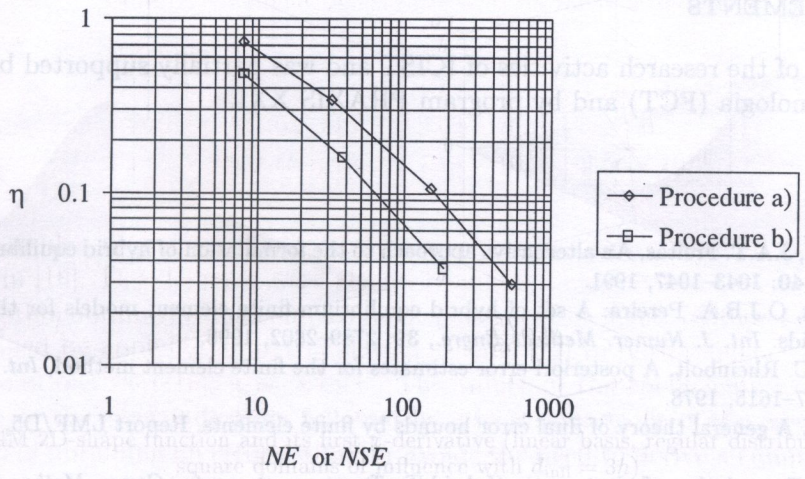

Fig. 7. Relative error for the different procedures

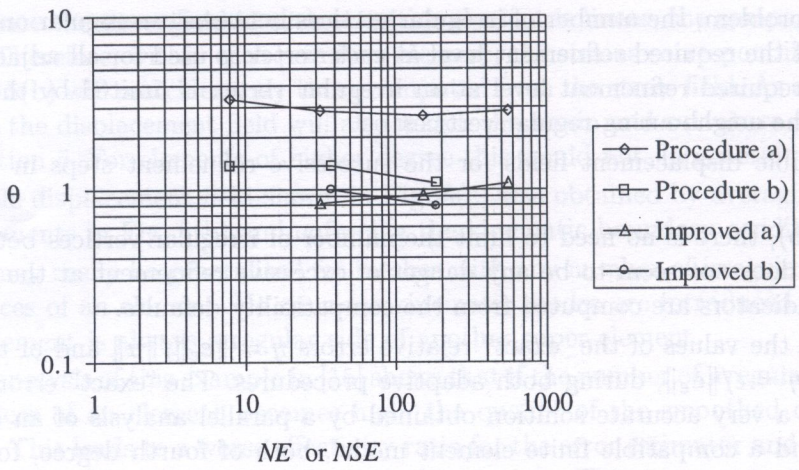

Fig. 8. Effectivity of the different estimators

13. Conclusions

Equilibrated solutions, locally satisfying all the equilibrium conditions, may be obtained by using hybrid equilibrium finite elements.

Compatibility defaults for *2D* and *3D* equilibrium elements have been proposed, together with a formula for an element error indicator based on these defaults. The compatibility defaults and, therefore, the error indicators are independent of the amplitudes of the spurious kinematic modes. These indicators may thus be used when the elements are not assembled into super-elements, provided that a solution exists for the initial mesh. The use of h-refinement ensures that a solution will always exist for each refined mesh. In *2D*, it appears that h-refinement does not cause additional spurious modes. Nevertheless, further work is required to evaluate appropriate coefficients for the error indicator, particularly in *3D*.

When super-elements are used, spurious kinematic modes are absent. Therefore, a compatible displacement field may be derived from the equilibrated solution. This technique provides both a compatible displacement field and an upper bound of the global error. This bound may be rather high, but an improved error estimate may be easily computed. The cause of the irregular refinement patterns that appeared when this method was previously used is now understood and can be avoided. Further investigations are required to extend the error indicators to higher degree elements and to the *3D* case.

Acknowledgements

This work is part of the research activities of ICIST and was partially supported by Fundação para a Ciência e a Tecnologia (FCT) and by program PRAXIS XXI.

References

[1] J.P.M. Almeida, J.A.T. Freitas, An alternative approach to the formulation of hybrid equilibrium finite elements. *Comp. Struct.*, **40**: 1043–1047, 1991.

[2] J.P.M. Almeida, O.J.B.A. Pereira. A set of hybrid equilibrium finite element models for the analysis of three-dimensional solids. *Int. J. Numer. Methods Engrg.*, **39**: 2789–2802, 1996.

[3] I. Babuska, W.C. Rheinbolt. A posteriori error estimates for the finite element method. *Int. J. Numer. Methods Engrg.*, **12**: 1597–1615, 1978.

[4] J.F. Debongnie. A general theory of dual error bounds by finite elements. Report LMF/D5, University of Liège, 1983.

[5] J.A.T. Freitas. Formulation of elastostatic Hybrid-Trefftz stress elements. *Comp. Meths. Appl. Mech. Engrg.*, **153**: 127–151, 1998.

[6] C. Johnson, B. Mercier. Some equilibrium finite element methods for two-dimensional elasticity problems. *Numer. Math.*, **30**: 103–116, 1978.

[7] D.W. Kelly, J.P.S.R. Gago, O.C. Zienkiewicz. A posteriori error analysis and adaptive processes in the finite element method: Part I – Error analysis. *Int. J. Numer. Methods Engrg.*, **19**: 1593–1619, 1983.

[8] P. Ladevèze, D. Leguillon. Error estimate procedure in the finite element method and applications. *SIAM J. Numer. Anal.*, **20**(3): 483–509, 1983.

[9] E.A.W. Maunder, J.P.M. Almeida. Hybrid-equilibrium elements with control of spurious kinematic modes. *Computer Assisted Mechanics and Engineering Sciences*, **4**: 587–605, 1997.

[10] A.J. May. *Error Bounding in Meshes of Triangular Equilibrium Super-Elements.* MSc Dissertation, Heriot-Watt University, Edinburgh, 1996.

[11] J.T. Oden, L. Demkowicz, W. Rachowicz, T.A. Westermann. Toward a universal h-p adaptive finite element strategy. Part 2. A posteriori error estimation. *Comp. Meths. Appl. Mech. Engrg.*, **77**: 113–180, 1989.

[12] O.J.B.A. Pereira. *Utilização de Elementos Finitos de Equilíbrio em Refinamento Adaptativo.* PhD Thesis, Technical University of Lisbon, 1996.

[13] O.J.B.A. Pereira, J.P.M. Almeida. Equilibrium finite elements and dual analysis in three-dimensional elastostatics. In: E.R.A. Oliveira, J. Bento, eds., *Education, Practice and Promotion of Computational Methods in Engineering*, 955–960. Techno-Press, Korea, 1995.

[14] O.J.B.A. Pereira, J.P.M. Almeida, E.A.W. Maunder. Adaptive methods and related issues from the viewpoint of hybrid equilibrium finite element models. In: P. Ladevèze, J.T. Oden, eds., *Advances in Adaptive Computational Methods in Mechanics*, 427–441. Elsevier Science, Amsterdam, 1998.

[15] O.J.B.A. Pereira, J.P.M. Almeida, E.A.W. Maunder. Adaptive methods for hybrid equilibrium finite element models. *Comput. Methods Appl. Mech. Engrg.*, **176**: 19–39, 1999.

[16] M.A. Piteri. *Geração de Malhas Hierárquicas em Domínios Bidimensionais e Tridimensionais.* PhD Thesis, Technical University of Lisbon, 1998.

[17] W. Prager, J.L. Synge. Approximations in elasticity based on the concept of function space. *Quart. Appl. Math.*, **5**(3): 241–269, 1947.

[18] B.M.F. de Veubeke. Upper and lower bounds in matrix structural analysis. *AGARDograf*, **72**: 165–201, 1964.

[19] B.M.F. de Veubeke. Diffusive equilibrium models. In: M. Geradin, ed., *B.M. Fraeijs de Veubeke Memorial Volume of Selected Papers*, 569–628. Sijthoff & Noordhoff, Alphen aan den Rijn, The Netherlands, 1980.

[20] B.M.F. de Veubeke, O.C. Zienkiewicz. Strain energy bounds in finite element analysis by slab analogy. *J. of Strain Analysis*, **2**(4): 265–271, 1967.

[21] H.G. Zhong, P. Beckers. Solution approximation error estimators for the finite element solution. Report SA-140, LTAS, University of Liège, January 1990.

[22] O.C. Zienkiewicz, J.Z. Zhu. A simple error estimator and adaptive procedure for practical engineering analysis. *Int. J. Numer. Methods Engrg.*, **24**: 337–357, 1987.

[23] O.C. Zienkiewicz, J.Z. Zhu. The Superconvergent Patch Recovery and a posteriori error estimates: Part 1 – The recovery technique; Part 2 – Error estimates and adaptivity. *Int. J. Numer. Methods Engrg.*, **33**: 1331–1382, 1992.